World Journal of Advanced Research and Reviews
eISSN: 2581-9615 CODEN (USA): WJARAI
Cross Ref DOI: 10.30574/wjarr
Journal homepage: https://wjarr.com/

(RESEARCH ARTICLE)

Check for updates

# Theoretical investigation of structural, electronic, optical and thermoelectric properties of $GaAgO_2$ based on Density Functional Theory (DFT): Two approach

Md. Rajib Munshi [1,*], Md. Zuel Rana [1], Sapan Kumar Sen [2], Md. Ruhul Amin Foisal [3] and Md. Hazrat Ali [4]

[1] *Department of Physics, Faculty of Science of Engineering, European University of Bangladesh, Gabtoli, Dhaka-1216, Bangladesh.*
[2] *Institute of Electronics, Atomic Energy Research Establishment, Bangladesh Atomic Energy Commission, Dhaka, Bangladesh.*
[3] *Department of Chemistry, Faculty of Science of Engineering, European University of Bangladesh, Gabtoli, Dhaka, Bangladesh.*
[4] *Department of Electrical and Electronic Engineering, Faculty of Science of Engineering, European University of Bangladesh, Gabtoli, Dhaka, Bangladesh.*

World Journal of Advanced Research and Reviews, 2022, 13(02), 279–291

Publication history: Received on 05 January 2022; revised on 09 February 2022; accepted on 11 February 2022

Article DOI: https://doi.org/10.30574/wjarr.2022.13.2.0130

## Abstract

In this research we have investigated systematically, the structural, electronic, bonding, optical, thermodynamic aspects of the $GaAgO_2$ crystal using first-principles computations based on the density functional theory (DFT). To begin, the bandgap energies of $GaAgO_2$ crystal have estimated to be 0.640 eV and 0.768 eV using the Generalized Gradient Approximation (GGA) based on the Perdew–Burke–Ernzerhof (PBE) and Revised Perdew–Burke–Ernzerhof (RPBE) functional methods. The density of state and partial density of state of $GaAgO_2$ were then simulated to determine the nature of the orbital of the Ga, Ag, and O atoms. The Mulliken population charge and electron density distributions have estimated to further elucidate the bonding nature of $GaAgO_2$. The complex dielectric function, refractive index, reflectivity, absorption coefficient, loss function, and photoconductivity of $GaAgO_2$ are all computed and analyzed in depth for the optical transitions. Additionally, come to the realization of it, the thermo-electronic and thermophysical features have been added to enable this crystal to absorb visible light and retain a stable thermal state, enabling them to be employed in optoelectronic devices such as lasers, solar cells, and even luminescence ones.

**Keywords:** Band gap; Electronic structure; DOS; PDOS; Optical; Thermodynamic properties

## 1. Introduction

Semiconductors materials have experienced significant extensive research in the past several decades, because of their distinct characteristics and potential industrial uses for which they hold great promise [1-2]. Recently, semiconductors have garnered considerable study attention owing to their exceptional thermal and chemical durability [3], as well as their unique structural, morphological, optical, and catalytic features [4-5]. It has immense applications in electronic technology [6], power devices [7], nanospintronic devices [8-9], transistors [10], photo-sensors [11], microcontrollers [12] and integrated circuits [13]. In the contemporary era, most of the electronic technologies and optoelectronic devices solely depend on using of semiconductor materials due to their chemical, physical, thermo-electronic properties [14], good chemical stability [15-16] and optical characters [17], gas sensing [18], environmental purification [19], therapeutic material [20], element in photovoltaic cells [21] and so on. Furthermore, due to their inexpensive cost and availability, modifications to their chemical structures have been developed to make them more environmentally

* Corresponding author: Md. Rajib Munshi
Department of Physics, Faculty of Science of Engineering, European University of Bangladesh, Gabtoli, Dhaka-1216, Bangladesh.

friendly and non-toxic [22–23] and liquid crystals have been developed for more flexible implementations in modern technologies [24-26]. Meanwhile, obtaining a high-efficiency semiconductor at room temperature utilizing group II–IV metals is a monumental constraint because to the variety of suitable moods [27-30]. Among these flaws, the atomic size, broad band gap, and low cost are the most important for developing novel semiconductor materials, despite the fact that they have a significant impact on the ability to absorb or emit ultraviolet (UV) light in optoelectronic applications [31-32]. Moreover, Gallium crystals or gallium oxides have been proved to be promising candidates for transparent electronics, chemical and gas sensors, optoelectronic devices and UV emitters with a large band gap [33-34] and in a variety of structural configurations the increased demand for silver-based alloys has prompted researchers to investigate and develop novel materials with acceptable thermochemical characteristics [35-37]. In accordance to these intentions Gallium oxide alloy including Ag metals with formula $GaAgO_2$ has been designed to investigate structural geometry, electronic structure, Mulliken population, electron charge density, optical and thermo-electronic properties Using computational methods. Although Ga and Ag atoms have been favored owing to their smaller atomic size, which facilitates electronic transitions from the valence band to the conduction band and the generation of a significant number of free electrons, oxygen creates more free electrons than Ga and Ag atoms in the $GaAgO_2$ crystal. The first principle technique has been used to conduct a systematic study of the structural geometry, electronic structure, Mulliken population, electron charge density, optical characteristics, thermo-electronic, properties of $GaAgO_2$ in this research. Finally, GGA with PBE and GGA with RPBE functional have been applied to perform a comparison investigation in order to acquire a more precise magnitude and acceptability of the compounds. It is anticipated that this research will significantly contribute to gaining a thorough understanding of this material and will serve as a guide for its applications.

## 2. Computational methods

The GGA with PBE is based on the CASTEP code from Material Studio version 17.1.0.48 has been used to calculate band structure, the total density of state (DOS) and the partial density of state (PDOS), because it is suspected to be the most accurate and reliable approach to find out electronic structure and structural features [38]. In this case, the density of state and band structure have been calculated using the cutoff at 510 eV and k point at 2×2×1 with norm-conserving pseudopotentials. The Electron charge density distribution, optical properties, such as reflectivity, absorption, refractive index, dielectric function, conductivity, and loss function, as well as thermoelectric properties such as enthalpy, heat capacity, entropy, specific heat, mechanical properties have all been simulated in the same way. Moreover, geometrical optimization is completed prior to energy calculations and the atom-force convergence threshold is set at 3×10-6 eV/A. The maximum displacement is at 1×10-3A and the total energy and the maximal stress are at 1×10-5 eV/atom and 5 × 10-2 GPa, respectively. The another common method, such as Generalized Gradient Approximation (GGA) with Revised Perdew–Burke–Ernzerhof functional (RPBE), also has been investigated using required cut-off energy at the same condition.

## 3. Results and discussion

### 3.1. Optimized structure

The lattice parameters are a = 3.03060 Å, b = 3.03060 Å, c = 12.36920 Å and angels between them are α = 90.000 Å, β = 90.000 Å, γ = 120.000 Å. The monoclinic $GaAgO_2$ crystal and the area cluster which is Hermanna Mauguin P63/mmc [194], hexagonal crystals system, point cluster 6/mmm, Hall-P 6c 2c, density 6.04 g/cm3 are shown in Figure 1(a) and 1(b).

### 3.2. Electronic structure

The Fermi level has been set to zero in order to determine the electronic band structures of $GaAgO_2$ using GGA with PBE and GGA with RPBE. As shown in Figure 2(a), between the K and M symmetry points, the minimum of conduction bands (MCB) is settled, while the maximum of valence bands (MVB) is sited at the H symmetry point. For $GaAgO_2$ utilizing GGA with PBE method, the symmetry point is observed at different MCB and MVB locations, which is referred to as the indirect band gap, with values obtained of 0.640 eV.

The highest levels of the valance band around the H symmetry point, on the other hand, are dispersive, although not as dispersive as the upper regions of $GaAgO_2$. Using a lower effective mass carrier, it is possible to identify materials that might be used in high-mobility electronic devices [39]. GGA with RPBE has been shown to calculate band gaps under the same conditions and the accompanying visual views are provided in Figure 2. (b), which demonstrates that the band gaps for $GaAgO_2$ are both indirect with magnitudes of 0.768. By analyzing the accompanying figures, it is plausible to

extrapolate that all band gaps for $GaAgO_2$ are deemed indirect band gap and the values are nearly identical for the two approaches. The comparison values for the optimum situation are shown in Table 1.

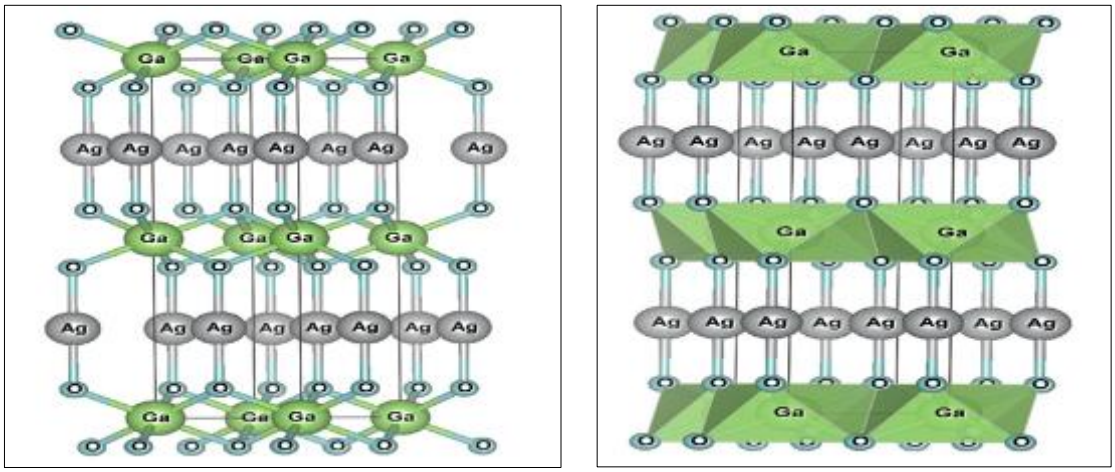


**Figure 1** (a) Structure of $GaAgO_2$ (Ball and stick) and (b) Structure of $GaAgO_2$ (Polyhedral)

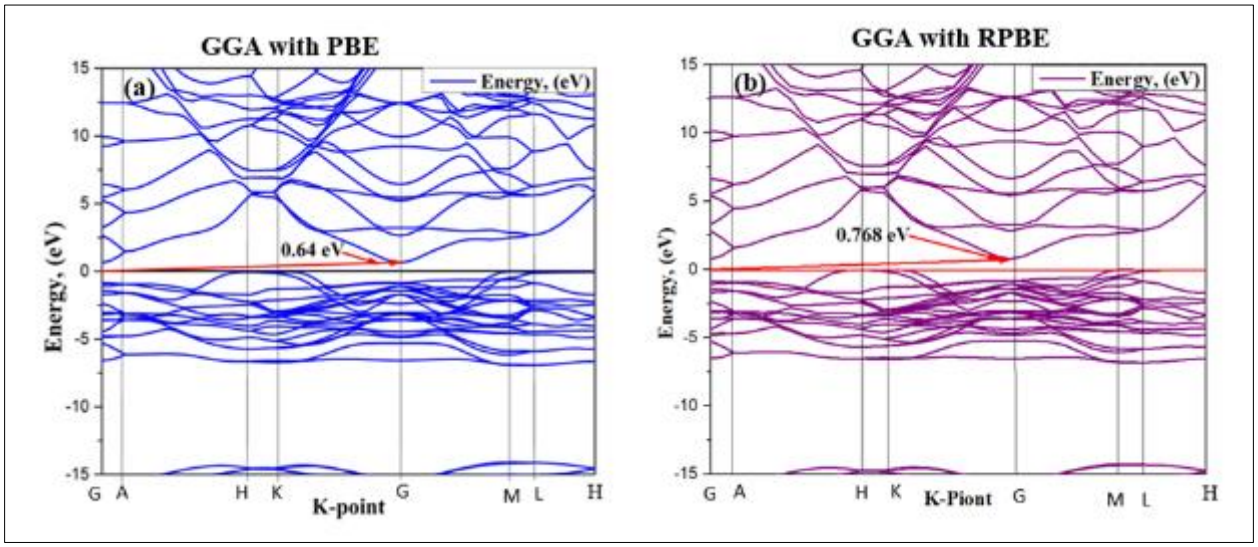


**Figure 2** (a, b) Electronic band structure of $GaAgO_2$ in GGA with PBE and GGA with RPBE method respectively

**Table 1** Comparative bandgaps for $GaAgO_2$

| Compound Name | Analysis Method | |
|---|---|---|
| $GaAgO_2$ | **GGA with PBE** | **GGA with RPBE** |
| | 0.640 eV | 0.768 eV |

### 3.3. Mulliken atomic population

To have a deeper understanding about the bonding properties of $GaAgO_2$, the Mulliken atomic population [40-41] is computed and listed in Table 2. Moreover, this research provides credible information on bond overlap and charge transfer between the various sorts of atoms in a material. As seen in Table 2, the Ga and Ag atoms have a positive charge, whereas the O atoms have a negative charge for the $GaAgO_2$ material. As a result, charge transfer occurs between Ga and Ag atoms and the O atom. Our computations are similar with those of prior theoretical investigations of a similar kind [42].

**Table 2** Population analysis of $GaAgO_2$ in GGA with PBE approach

| Analysis | Mulliken | | | | | | | | | Hirsfeld |
|---|---|---|---|---|---|---|---|---|---|---|
| Compound | Species | s | p | d | Total | Charge (e) | Bond | Population | Lengths (Å) | Charge (e) |
| $GaAgO_2$ | Ga | 0.56 | 0.95 | 10.00 | 11.51 | 1.49 | O - Ga | 0.75 | 2.0105 | 0.45 |
| | Ag | 2.70 | 6.31 | 9.81 | 18.82 | 0.18 | O - Ag | 0.27 | 2.1019 | 0.28 |
| | O | 1.84 | 5.00 | 0.00 | 6.84 | - 0.84 | | | | - 0.36 |

### 3.4. Density of states and partial density of state

The DOS and PDOS have been used to investigate the properties of electronic band structures and orbital dispersion. The DOS and PDOS of Ga, Ag, and O elements have been determined for $GaAgO_2$ crystals using the GGA with PBE and GGA with RPBA approach. Figure 3(a, b) and 3 (c, d) depicts the simulation of DOS and PDOS for $GaAgO_2$ in GGA with PBE and GGA with RPBA approach. The nature of $3d^{10}$, $4s^2$ and $4p^1$ for Ga; $4p^6$, $4d^{10}$ and $5s^1$ for Ag; and $2s^2$ and $2p^4$ for O elements have been studied to explain the transition of electrons due to hybridization by traveling from the maximum valence band (MCB) to the minimum conduction band (MCB). The p-orbital dominates the conduction band, while the d-orbital contributes the most to the formation of the valance band. The $4p^1$ orbital is almost vacant in Ga, which causes it to migrate toward the conduction band; nevertheless, the p-orbital is partly filled by $2p^4$ orbitals for O-atoms and $4d^{10}$ and $5s^1$ orbitals for Ag-atoms. As a consequence, the conduction band's greatest peak for PDOS is obtained from the combined contribution of p-orbital at around 2.4 eV and s-orbital at approximately 5.7 eV. Additionally, the PDOS of p-orbitals in the conduction band is identical to the DOS pattern. As a consequence, the conduction band is composed of $4p^1$ Ga, $4d^{10}$ and $5s^1$ of Ag and $2p^4$ O-atoms, while the valence band is composed of a combination of p- and d-orbitals. The maximum electron intensity or density in the valence band is around 13.0 electrons/eV, while d-orbital electrons account for almost 8.4 electrons/eV and p orbital accounts for 4.6 electrons/eV. The s-orbital and p-orbital have a higher electron density in the conduction band.

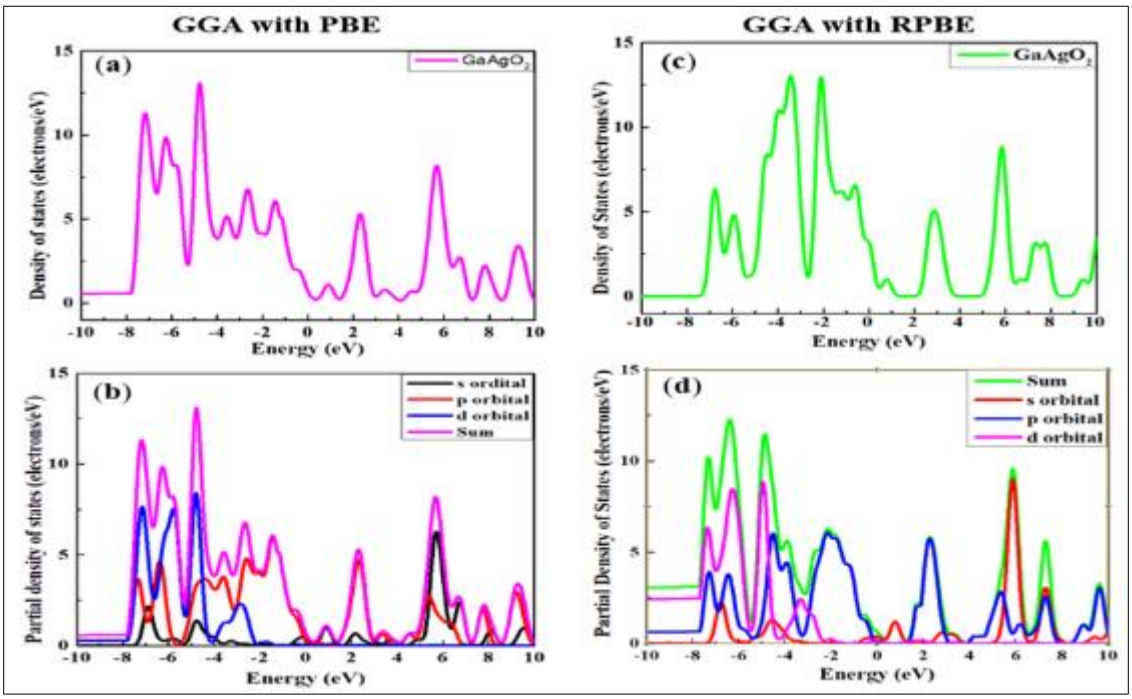

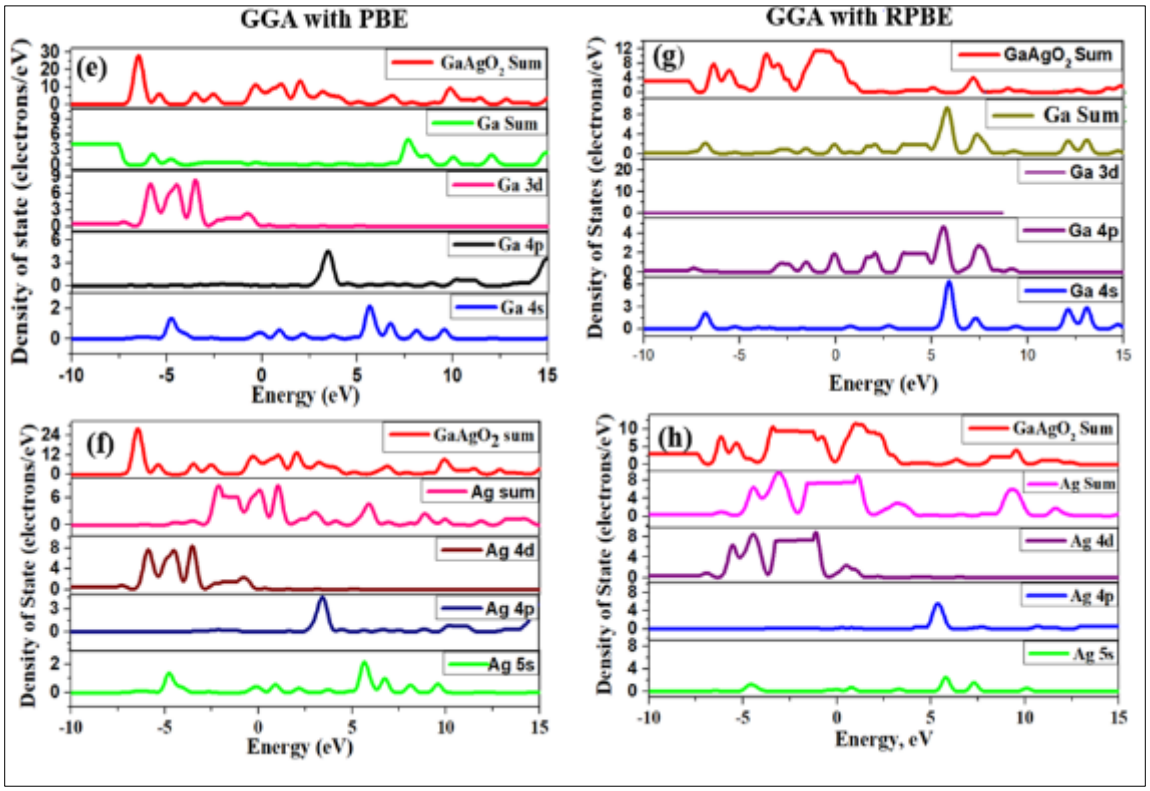


**Figure 3 (a, b**) Total DOS and PDOS of $GaAgO_2$ in GGA with PBE method (c, d) Total DOS and PDOS of $GaAgO_2$ in GGA with RPBE method (e, f) PDOS of $GaAgO_2$ for Ga and Ag atom in GGA with PBE method (g, h)) PDOS of $GaAgO_2$ for Ga and Ag atom in GGA with RPBE method

### 3.5. Electron charge density

The electron charge density distribution of $GaAgO_2$ crystal provide valuable information about its chemical bonding characteristics. Hence we determined the charge density map of $GaAgO_2$ in 3D visualization and along (100) plane using GGA with PBE and GGA with RPBE approach and illustrated the result in fig 4(a, b) and (c, d). The electron charge density distribution of the $GaAgO_2$ crystal reveals important details regarding its chemical bonding properties. It is generally recognized that when the electron clouds of two atoms overlap and the electrons consolidate in the overlapping region, a covalent bond is formed between them. There is indeed a significant overlap of electron clouds between Ga and O atoms in the figure, which validates the existence of sigma type Ga-O covalent bonds in $GaAgO_2$. There is no overlapping of charge distribution among Ag atoms viewing the ionic character of Ag - Ag bond. The ionic nature is the consequence of the metallic character [43] showing the metallic feature of Ag - Ag Bonds Overall, the investigation of the density of states, Mulliken atomic population, and the total charge density of $GaAgO_2$ is comprehensive.

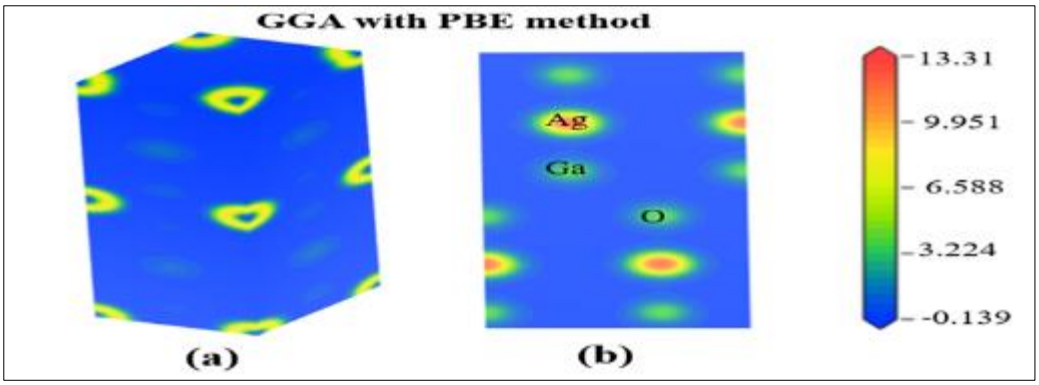

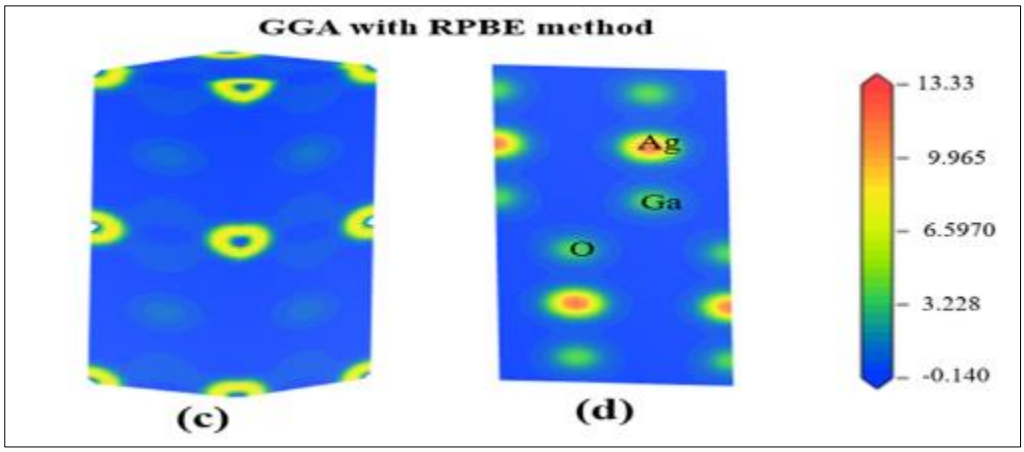


**Figure 4** Electronic charge density (a) 3 D View and (b) along 100 plane of $GaAgO_2$ (c) 3 D View and (d) along 100 plane of $GaAgO_2$

### 3.6. Optical properties

Indeed, optical characteristics of solids are a valuable tool for studying energy band structure, excitations, impurity levels, localized defects, and lattice vibrations, among other things. To prosecute the optical properties of $GaAgO_2$ crystals absorption, refractive index, dielectric function ε (ω), optical conductivity, and loss function have been explored. Reflectivity, absorption, refractive index, dielectric function ε(ω), optical conductivity, and loss function have all been depicted in such studies. The complex conductivity or frequency-dependent complex dielectric function ε(ω), is intimately connected to the energy band structure of solids.

*3.6.1. Optical reflectivity*

However, since electron delocalization processes can lead to an insulator-to-metal transition, the formation of periodically spaced vacancy layers inside the meta-stable phase of Ga-Ag-$O_2$ phase-change materials has recently been getting a lot of attention. Several earlier investigations have shown that a lower reflectivity corresponds to a greater UV or visible light absorption [44–45]. In Figure 5(a) the optical reflectivity is illustrated in GGA with PBE method and it is seen that the reflectivity of $GaAgO_2$ starts at around 0.32 from the initial frequency. Afterwards the the reflectivity of $GaAgO_2$ changes roughly before 2.5 eV and gradually increased after 2.5 eV. In addition, for $GaAgO_2$ reflectivity increases to about 0.47 and then starts to fall for the corresponding frequency at about 3.8 eV. In Figure 5(b) the optical reflectivity is illustrated in GGA with RPBE method and from Figures 5(a) and 5(b), it is observed that the value of reflectivity is highly lower compared to the absorption.

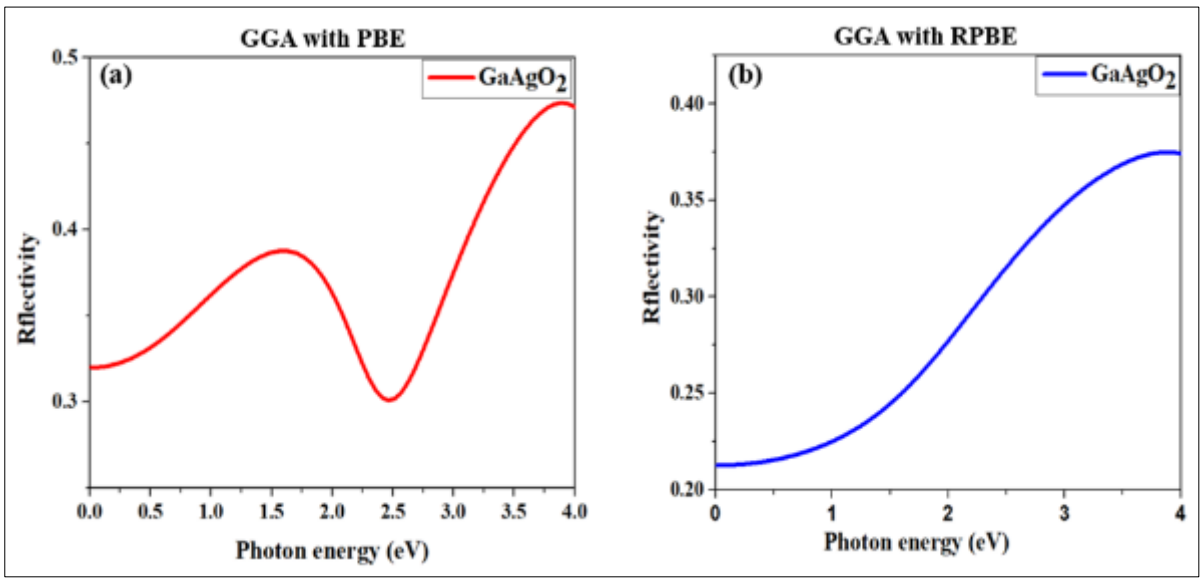


**Figure 5** Optical reflectivity of $GaAgO_2$ (a) GGA with PBE and (b) GGA with RPBE methods

*3.6.2. Absorption*

The polycrystalline polarization technique has been used to compute the optical absorbance of $GaAgO_2$, and a modest smearing value of 0.1 was used to obtain more distinct absorbance peaks. Figure 6(a) the absorption peak of $GaAgO_2$ in GGA with PBE method shows that absorbance peaks are created at various photon energies where electronic transitions from MVB to MCB occur as a result of incident light (visible). In this case, the absorption increases slowly from 0.5 to 2.0 eV and then decreases unto 2.5eV and increases dramatically after that. In Figure 6(b) the absorption peak has shown in GGA with RPBE method. As this $GaAgO_2$ material has a reduced band gap and better absorption, as well as a wide range of photon energy absorption capabilities soon after the beginning point, it might be employed to make various optical communication and optoelectronic device applications devices [46-47].

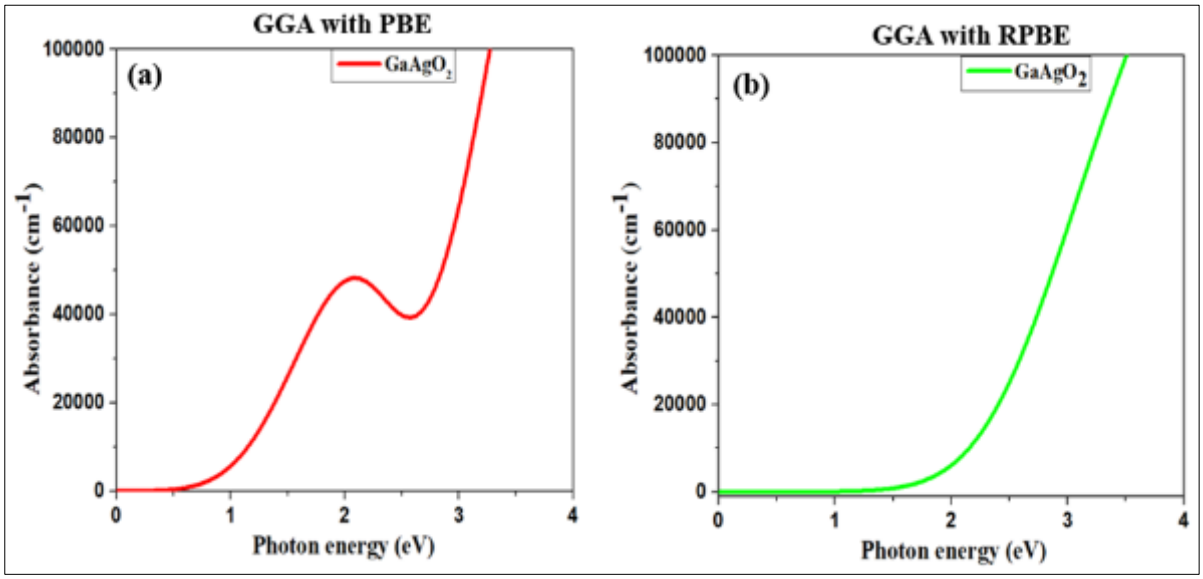


**Figure 6** Optical absorption of $GaAgO_2$ (a) GGA with PBE and (b) GGA with RPBE methods

*3.6.3. Refractive Index*

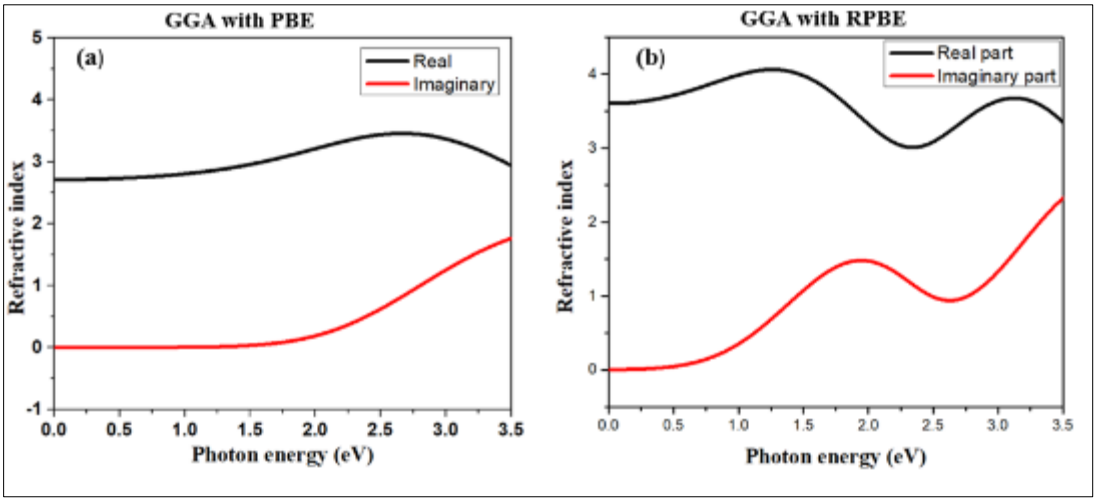


**Figure 7** Refractive index of $GaAgO_2$ (a) GGA with PBE and (b) GGA with RPBE methods

The refractive index, which refers to the relationship between the speed of light in a vacuum and the speed of light in another medium, implies that a greater refractive index indicates a denser material or less absorption. In Figure 7(a), the refractive index as a function of photon energy seems to have been determined using the GGA with PBE approach. It is composed of two components: real and imaginary, and may be defined as the ratio of the speed of light in free space to the speed of light in another medium. The greater the value of the real component, the more suitable it is for use in optoelectronic devices; conversely, the greater the value of the imaginary portion, the less suitable it is for use in

optoelectronic devices. The refractive index of $GaCuO_2$ is greater in the real portion at the origin of photon energy, but the imaginary part is nearly zero. The real parts of the refractive index follow a rather steady pattern with rising photon energy up to 2.75 eV, after which they gradually drop with increasing photon energies. The refractive index as a function of photon energy has been seen another common method GGA with RPBE in figure 7(b).

*3.6.4. Dielectric function*

For investigating the optical characteristics of a material the dielectric function is the most influential tool, which are connected with adsorption properties for solids as indicated in the following equation: $(\omega) = \varepsilon_1(\omega) + i\varepsilon_2(\omega)$, Here, $\varepsilon_1(\omega)$ and $\varepsilon_2(\omega)$ are represented the dielectric constant (real part) and the dielectric loss factor (imaginary part), respectively. The dielectric function is associated with the physical space of materials that are physically compatible with absolute permittivity or permittivity. The real component of the dielectric function represents the capacity of dielectric materials to store energy in an electric field, while the imaginary part represents the ability of dielectric materials to dissipate energy. The dielectric properties of $GaAgO_2$ crystals in GGA with PBE and GGA with RPBE are shown in Figure 8(a, b). It is clear that, for $GaAgO_2$ crystals, the real parts of the dielectric function illustrate the larger magnitude than imaginary part meaning that it can be highly used as an electrostatic cell as energy storage materials.

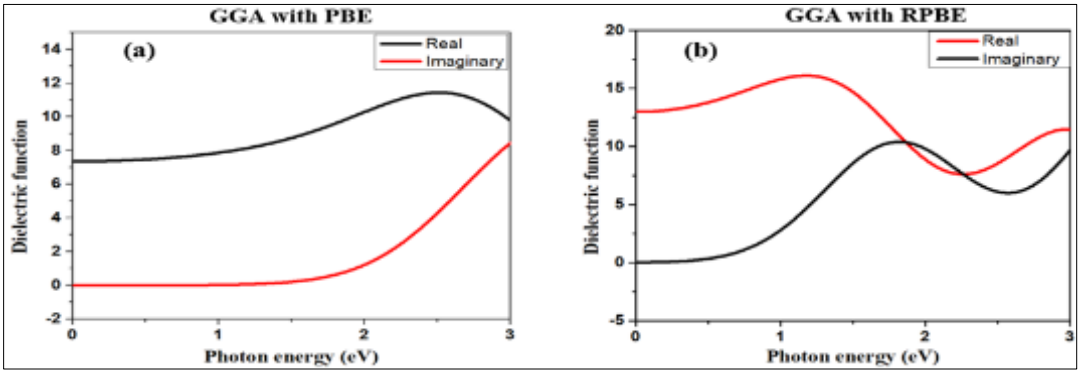


**Figure 8** Refractive index of $GaAgO_2$ (a) GGA with PBE and (b) GGA with RPBE methods

*3.6.5. Conductivity*

Conduction in semiconductors based on energy bands and orbital electrons is related to the distinct orbital space of electrons. In semiconductors, conduction occurs as a result of the existence of holes and free electrons in the crystal molecules. Figure 9(a, b) demonstrates that the conductivity of $GaAgO_2$ material in GGA with PBE and GGA with RPBE method. The real parts increase slowly up to 2.5 eV and after then increase sharply whereas the imaginary parts decrease following opposite direction with little variation at the end portion. It is also observed that the upper peak of the conductivity reaches about 6.77 1/fs at 3.6 eV for of $GaAgO_2$. Finally, it was rebuilding that $GaAgO_2$ crystal has a good conductivity.

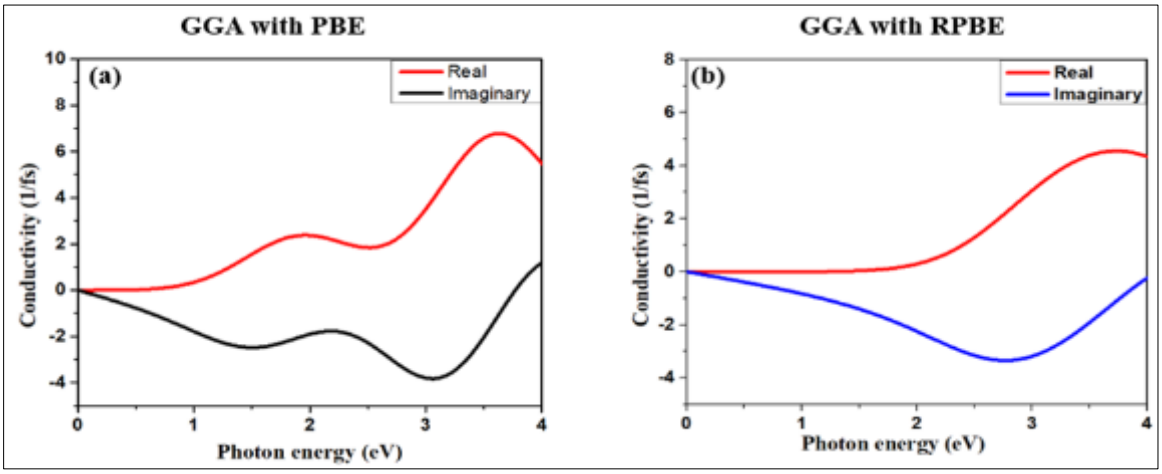


**Figure 9** Conductivity of $GaAgO_2$ (a) GGA with PBE and (b) GGA with RPBE methods

*3.6.6. Loss function*

The energy curve is used to establish the zones of high and low energy. The first region accounts for the large energy loss with frequency or spectrum shift after an ionizing edge, sometimes referred to as the oxidation state of d-orbital splitting for atomic metals in complex compounds with a range higher than 3.5 eV. The other is a low energy loss function with an energy loss of less than 3.0 eV that may be used to determine the composition and electronic structure of a material. The loss function for $GaAgO_2$ crystals is shown in figure 10(a) for GGA with PBE and 10(b) for GGA with RPBE. As seen in the figure, $GaAgO_2$ has a higher energy loss in the low energy zone due to its electronic structure and composition. On the other hand, the loss function in the higher energy region steadily rose, indicating that there is no difference in d-orbital splitting.

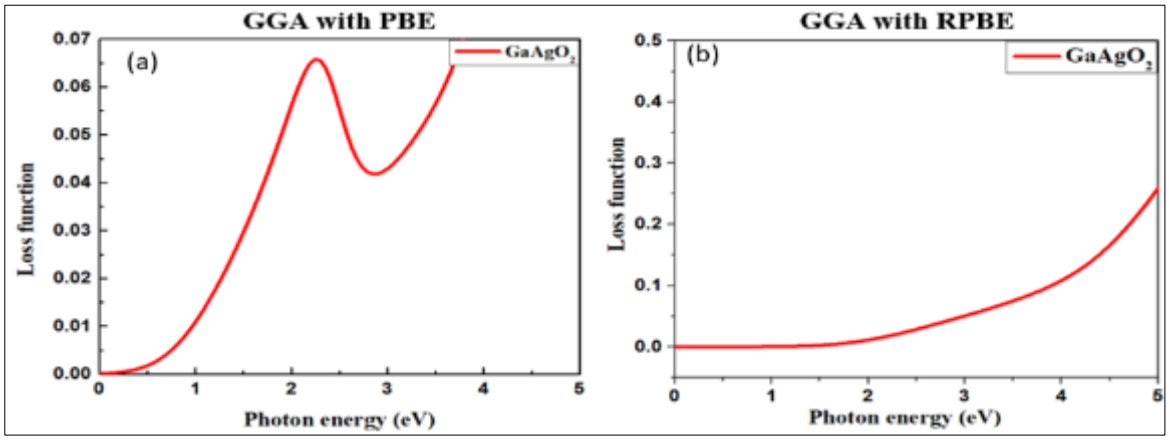


**Figure 10** Loss function of $GaAgO_2$ (a) GGA with PBE and (b) GGA with RPBE methods

### 3.7. Thermoelectric Properties

Thermoelectric features include heat transfer through electronic transitions in physical and chemical processes [48], energy transfer via biological and chemical processes [49], and system-environment interaction. The fundamental concepts of thermodynamics are entropy, heat capacity, enthalpy, and free energy, which enable the interaction of physics and physical chemistry in every system. According to Petersen et al., entropy and enthalpy are tightly related, and entropy provides information on a substance's discharge state. Figure 11(a, b) illustrates the total comparison of thermophysical properties of $GaAgO_2$ in GGA with PBE and GGA with RPBA methods.

*3.7.1. Entropy*

Entropy is a significant concept in physics and chemistry, as well as in a variety of other fields of study. It is a component of cosmology and economics, as well as a key component of thermodynamics and physical chemistry. It is a metric for the dysfunctional state of a system. Additionally, it gives the one-of-a-kind property of a thermodynamic system, in which the value fluctuates in proportion to the quantity of matter present. Entropy is commonly symbolized by the letter S in equations (1) and (2) and has units of joules per Kelvin ($J\ K^{-1}$) or $kg\ m^2\ S^{-2}\ K^{-1}$. A highly ordered system has low entropy. Figure 11 (a, b) shows the Entropy of $GaAgO_2$ in GGA with PBE and GGA with RPBE method. From figure 10(a) it is clear that at 1000 K, with the highest upper entropy at 1.28 eV for $GaAgO_2$. It has been demonstrated that increasing the temperature increases the entropy of $GaAgO_2$ crystals. As a result, it is possible to assert that the $GaAgO_2$ material exhibits less disordered behavior or molecular disruptions.

*3.7.2. Heat capacity*

The heat capacity of a body is the amount of energy necessary to increase its temperature by a certain amount. The current force has an effect on a material's heat capacity, which complicates the calculation of a material's kinetic energy. Thermal properties of an alloy might be significantly different from those of its individual components. As seen in Figure 11(c) in GGA with PBE method, total heat capacity of $GaAgO_2$ has improved gradually since its inception, making it an outstanding material for optoelectronic devices. The heat capacity in GGA with RPBE technique has been illustrated in 11(d).

*3.7.3. Enthalpy*

Enthalpy is a thermodynamic feature that relates to both the capacity for non-mechanical work and the capacity for heat release. The enthalpy is calculated using the following formula.

$$H = E + PV \quad \ldots\ldots\ldots\ldots\ldots \quad (1)$$
$$dH = TdS + PdV \ldots\ldots\ldots\ldots (2)$$

Here, H is enthalpy, E is the internal energy of the system, P is pressure and V is volume. From The enthalpy of $GaAgO_2$ in GGA with PBE and $GaAgO_2$ in GGA with RPBE method have illustrated in figure 11 (a, b) and it is found that with increasing the temperature from 100 to 1000 K, the change of enthalpy obtained from zero to 3.22 eV respectively, for the $GaAgO_2$.

*3.7.4. Free Energy*

The quantity of internal energy in a thermodynamic system that may be used to do work is referred to as free energy. the thermodynamic properties like free energy of $GaAgO_2$ have been listed in Figure 11(a, b) in GGA with PBE and GGA with RPBE methods. Finally, in our research, we discovered that the free energy of $GaAgO_2$ begins at the energy level zero eV at 100 K. The free energy gradually decreased with increase of temperature and maximum lower free energy obtained 1.92 eV at 1000 k. It could be concluded that the thermophysical properties such as entropy, heat capacity, enthalpy, and free energy of $GaAgO_2$ at different temperatures have been compared in Tables 3.

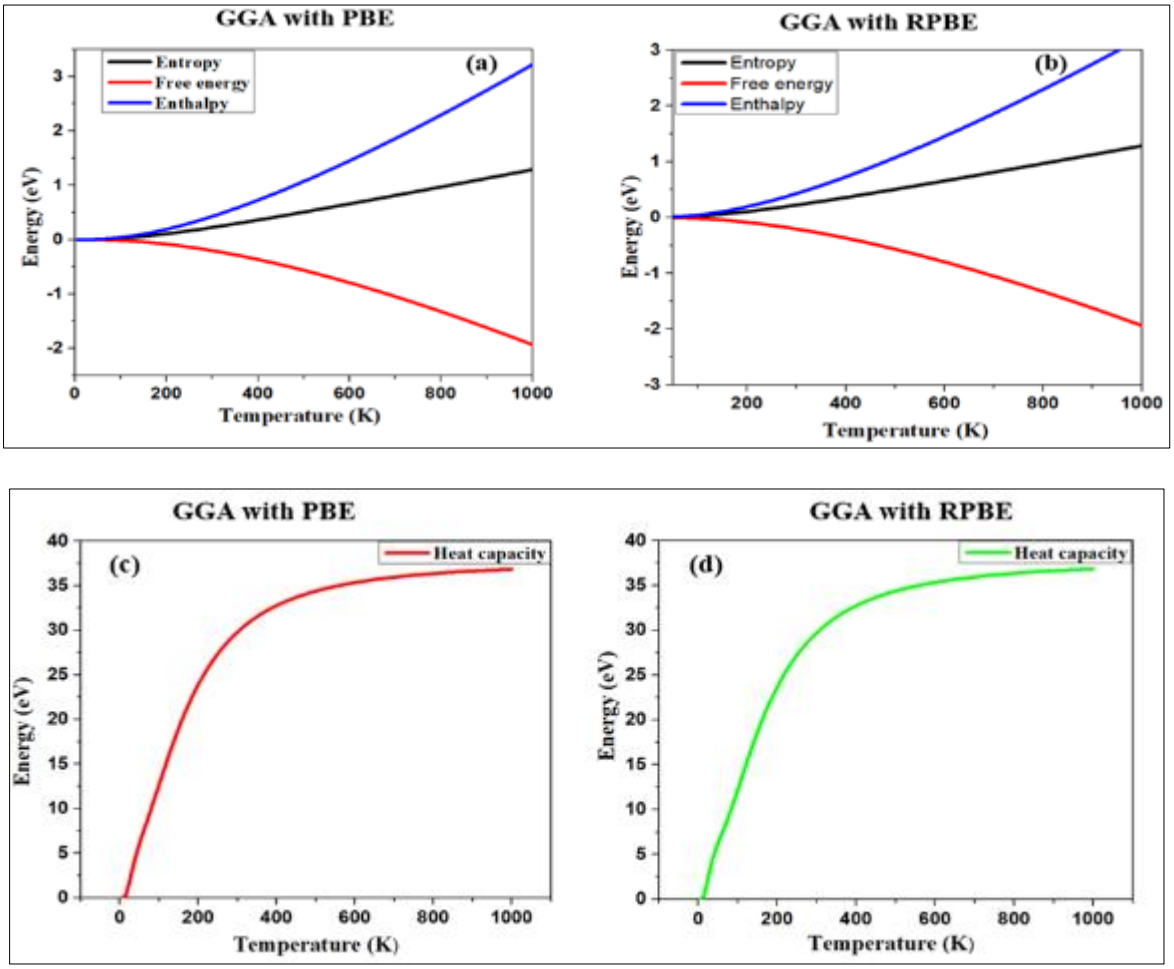


**Figure 11 (a, b)** Thermodynamic properties of $GaAgO_2$ in GGA with PBE and) GGA with RPBA methods comparison, (c, d) Total heat capacity

**Table 3** Thermophysical properties of $GaAgO_2$ at different temperatures in GGA with PBE method

| Compound Name | Temperature (K) | Entropy (eV/ K) | Heat capacity (eV/K) | Enthalpy (eV/K) | Free Energy (eV/K) |
|---|---|---|---|---|---|
| $GaAgO_2$ | 105.50 | 0.027 | 15.108 | 0.040 | -0.013 |
| | 276.36 | 0.196 | 27.185 | 0.358 | -0.162 |
| | 407.02 | 0.357 | 29.477 | 0.722 | -0.364 |
| | 597.97 | 0.607 | 30.674 | 1.361 | -0.753 |
| | 798.98 | 0.877 | 31.157 | 2.130 | -1.252 |
| | 1000 | 1.150 | 31.384 | 2.970 | -1.820 |

## 4. Conclusion

On the basis of density function theory, we have estimated extensive physical properties of $GaAgO_2$ CASTEP code, including structural, electrical, chemical bonding, optical, thermodynamic properties. The estimated lattice parameters accord well with each other. While gallium crystals or oxides have been developed as a material with a large band gap for use in optoelectronic devices, it has revealed that $GaAgO_2$ has been assessed as a material with a narrow band gap. Initially, utilizing GGA and the PBE method, a band gap of 0.640 eV has been obtained. Second, a functional analysis of GGA with RPBE was done for comparative purposes, yielding a value of 0.768 eV. The electronic band gap is smaller, as shown by changes in DOS and PDOS data, but the total sum of DOS is considerably bigger. As a consequence, GGA with PBE and GGA with RPBE have a closer band gap. The Mulliken atomic populations and total charge density demonstrate that all of the compounds have ionic, covalent, and metallic bonds. The absorption quality is excellent in visible and UV. However, the entropy and free energy values for $GaAgO_2$ are somewhat inverted, indicating a chemically and thermally less stable crystal at high temperatures. According to the definitive proof of absorption, reflectivity, loss function, and conductivity, $GaAgO_2$ is the best material to use in optoelectronic devices.

## Compliance with ethical standards

### *Acknowledgments*

This research received no specific grant from any funding agency in the public, commercial or not-for-profit sectors. I would like to thank the European University of Bangladesh (EUB) for its continuous support in the field of engineering and technological research.

### *Disclosure of conflict of interest*

The authors hereby declare there is no conflict of interest.

## References

[1] Dietl T. A ten-year perspective on dilute magnetic semiconductors and oxides. Nature materials. Dec 2010; 9(12): 965-74.

[2] Meyer J, Hamwi S, Kröger M, Kowalsky W, Riedl T, Kahn A. Transition metal oxides for organic electronics: energetics, device physics and applications. Advanced materials. 23 Oct 2012; 24(40): 5408-27.

[3] Alizadeh S, Hassanzadeh-Tabrizi SA. MoO3 fibers and belts: Molten salt synthesis, characterization and optical properties. Ceramics International. 1 Nov 2015; 41(9): 10839-43.

[4] Cai L, Rao PM, Zheng X. Morphology-controlled flame synthesis of single, branched, and flower-like α-MoO3 nanobelt arrays. Nano letters. 9 Feb 2011; 11(2): 872-7.

[5] Haber J, Lalik E. Catalytic properties of MoO3 revisited. Catalysis today. 17 Jan 1997; 33(1-3): 119-37.

[6] Davis EA, Mott N. Conduction in non-crystalline systems V. Conductivity, optical absorption and photoconductivity in amorphous semiconductors. Philosophical magazine. 1 Nov 1970; 22(179): 0903-22.

[7] Hudgins JL, Simin GS, Santi E, Khan MA. An assessment of wide bandgap semiconductors for power devices. IEEE Transactions on power electronics. 13 May 2003; 18(3): 907-14.

[8] Huang X, Makmal A, Chelikowsky JR, Kronik L. Size-dependent spintronic properties of dilute magnetic semiconductor nanocrystals. Physical review letters. 13 Jun 2005; 94(23): 236801.

[9] Awschalom DD, Flatté ME. Challenges for semiconductor spintronics. Nature physics. Mar 2007; 3(3): 153-9.

[10] Fortunato E, Barquinha P, Martins R. Oxide semiconductor thin-film transistors: a review of recent advances. Advanced materials. 12 Jun 2012; 24(22): 2945-86.

[11] Chilla JL, Butterworth SD, Zeitschel A, Charles JP, Caprara AL, Reed MK, Spinelli L. High-power optically pumped semiconductor lasers. In Solid State Lasers XIII: Technology and Devices. 8 Jul 2004; 5332: 143-150.

[12] Drury J, Fanderclai T, Linton F. CHI 99 SIG: automated data collection for evaluating collaborative systems. ACM SIGCHI Bulletin. 1 Oct 1999; 31(4): 49-51.

[13] Baeg KJ, Caironi M, Noh YY. Toward printed integrated circuits based on unipolar or ambipolar polymer semiconductors. Advanced Materials. 2013 Aug 21;25(31):4210-44.

[14] Dong J, Li J, Yang L, Zhang T, Lu R, Li J, Zhang L, Zhou S. Decoupling of thermo-electronic effect by traveling photothermal mirror method for characterization of thermal properties of semiconductors. Applied Physics Letters. 2020 Mar 16;116(11):114102.

[15] Smith AM, Duan H, Rhyner MN, Ruan G, Nie S. A systematic examination of surface coatings on the optical and chemical properties of semiconductor quantum dots. Physical Chemistry Chemical Physics. 2006;8(33):3895-903.

[16] Enengl C, Enengl S, Havlicek M, Stadler P, Glowacki ED, Scharber MC, White M, Hingerl K, Ehrenfreund E, Neugebauer H, Sariciftci NS. The role of heteroatoms leading to hydrogen bonds in view of extended chemical stability of organic semiconductors. Advanced Functional Materials. 2015 Nov;25(42):6679-88.

[17] Enengl C, Enengl S, Havlicek M, Stadler P, Glowacki ED, Scharber MC, White M, Hingerl K, Ehrenfreund E, Neugebauer H, Sariciftci NS. The role of heteroatoms leading to hydrogen bonds in view of extended chemical stability of organic semiconductors. Advanced Functional Materials. 2015 Nov;25(42):6679-88.

[18] Deki S, Beleke AB, Kotani Y, Mizuhata M. Liquid phase deposition synthesis of hexagonal molybdenum trioxide thin films. Journal of Solid State Chemistry. 2009 Sep 1;182(9):2362-7.

[19] Paul M, Dhanasekar M, Bhat SV. Silver doped h-MoO3 nanorods for sonophotocatalytic degradation of organic pollutants in ambient sunlight. Applied Surface Science. 2017 Oct 1; 418:113-8.

[20] Hu X, Li F, Xia F, Guo X, Wang N, Liang L, Yang B, Fan K, Yan X, Ling D. Biodegradation-mediated enzymatic activity-tunable molybdenum oxide nanourchins for tumor-specific cascade catalytic therapy. Journal of the American Chemical Society. 2019 Dec 27;142(3):1636-44.

[21] Mai LQ, Hu B, Chen W, Qi YY, Lao CS, Yang RS, Dai Y, Wang ZL. Lithiated MoO3 nanobelts with greatly improved performance for lithium batteries. Advanced Materials. 2007 Nov 5;19(21):3712-6.

[22] Someya T, Pal B, Huang J, Katz HE. Organic semiconductor devices with enhanced field and environmental responses for novel applications. MRS bulletin. 2008 Jul;33(7):690-6.

[23] Yang D, Ma D. Development of organic semiconductor photodetectors: from mechanism to applications. Advanced Optical Materials. 2019 Jan;7(1):1800522.

[24] Samuel ID, Turnbull GA. Organic semiconductor lasers. Chemical reviews. 2007 Apr 11;107(4):1272-95.

[25] Zhang W, Schneider J, Chigrinov VG, Kwok HS, Rogach AL, Srivastava AK. Optically addressable photoaligned semiconductor nanorods in thin liquid crystal films for display applications. Advanced Optical Materials. 2018 Aug;6(16):1800250.

[26] Ozaki M, Yoneya M, Shimizu Y, Fujii A. Carrier transport and device applications of the organic semiconductor based on liquid crystalline non-peripheral octaalkyl phthalocyanine. Liquid Crystals. 2018 Dec 8;45(13-15):2376-89.

[27] Nozik AJ, Memming R. Physical chemistry of semiconductor− liquid interfaces. The Journal of Physical Chemistry. 1996 Aug 1;100(31):13061-78.

[28] Addamiano A. Preparation and Photoluminescence of Silicon Carbide Phosphors Doped with Group III a Elements and/or Nitrogen. Journal of The Electrochemical Society. 1966 Feb 1;113(2):134.

[29] Kawazoe H, Yasukawa M, Hyodo H, Kurita M, Yanagi H, Hosono H. P-type electrical conduction in transparent thin films of CuAlO2. Nature. 1997 Oct;389(6654):939-42.

[30] McMahon MI, Nelmes RJ. New Structural Systematics in the II–VI, III–V, and Group-IV Semiconductors at High Pressure. physica status solidi (b). 1996 Nov 1;198(1):389-402.

[31] Kim M, Seo JH, Singisetti U, Ma Z. Recent advances in free-standing single crystalline wide band-gap semiconductors and their applications: GaN, SiC, ZnO, β-Ga2O3, and diamond. Journal of Materials Chemistry C. 2017;5(33):8338-54.

[32] Aziz SB. Modifying poly (vinyl alcohol) (PVA) from insulator to small-bandgap polymer: A novel approach for organic solar cells and optoelectronic devices. Journal of Electronic Materials. 2016 Jan 1; 45(1): 736-45.

[33] Ali M, Islam MJ, Rafid M, Ahmed R, Jeetu M, Rayhan R, Roy R, Chakma U, Kumer A. The computational screening of structural, electronic, and optical properties for SiC, Si0. 94Sn0. 06C, and Si0. 88Sn0. 12C lead-free photovoltaic inverters using DFT functional of first principle approach. Eurasian Chemical Communications. 1 May 2021; 3(5): 32738.

[34] Sen SK, Jalil MA, Hossain M, Manir MS, Hoque K, Islam MA, Hossain MN. Silver incorporated α-MoO3 nanoplates to nanorods: Exploring the effects of doping on structural, morphological and optical properties. Materials Today Communications. 1 Jun 2021; 27: 102404.

[35] Volkovich VA, Maltsev DS, Yamshchikov LF, Chukin AV, Smolenski VV, Novoselova AV, Osipenko AG. Thermodynamic properties of uranium in gallium–aluminium based alloys. Journal of Nuclear Materials. 1 Oct 2015; 465: 153-60.

[36] Shubin AB, Shunyaev KY, Yamshchikov LF. The diffusion of gallium into copper-tin alloy particles. In Defect and Diffusion Forum. 2009; 283: 238-242.

[37] Ramanujam J, Singh UP. Copper indium gallium selenide based solar cells–a review. Energy & Environmental Science. 2017; 10(6): 1306-19.

[38] Howlader D, Hossain MS, Chakma U, Kumer A, Islam MJ, Islam MT, Hossain T, Islam J. Structural geometry, electronic structure, thermo-electronic and optical properties of GaCuO2 and GaCu0. 94Fe0. 06O2: a first principle approach of three DFT functionals. Molecular Simulation. 22 Nov 2021; 47(17): 1411-22.

[39] Elfiky AA. SARS-CoV-2 RNA dependent RNA polymerase (RdRp) targeting: An in silico perspective. Journal of Biomolecular Structure and Dynamics. 13 Jun 2021; 39(9): 3204-12.

[40] Mulliken RS. Electronic population analysis on LCAO–MO molecular wave functions. II. Overlap populations, bond orders, and covalent bond energies. The Journal of Chemical Physics. Oct 1955; 23(10): 1841-6.

[41] Sanchez-Portal D, Artacho E, Soler JM. Projection of plane-wave calculations into atomic orbitals. Solid State Communications. 1 Sep 1995; 95(10): 685-90.

[42] Rahaman MZ, Rahman MA. ThCr2Si2-type Ru-based superconductors LaRu2M2 (M= P and As): An ab-initio investigation. Journal of Alloys and Compounds. 25 Feb 2017; 695: 2827-34.

[43] Singh RP. First principle study of structural, electronic and thermodynamic behavior of ternary intermetallic compound: CeMgTl. Journal of Magnesium and Alloys. 1 Dec 2014; 2(4): 349-56.

[44] Ferrari AM, Orlando R, Rérat M. Ab initio calculation of the ultraviolet–visible (UV-vis) absorption spectrum, electron-loss function, and reflectivity of solids. Journal of chemical theory and computation. 14 Jul 2015; 11(7): 3245-58.

[45] Kurt P, Banerjee D, Cohen RE, Rubner MF. Structural color via layer-by-layer deposition: layered nanoparticle arrays with near-UV and visible reflectivity bands. Journal of Materials Chemistry. 2009;19(47): 8920-7.

[46] Duy TN, Meslage J, Pichard G. CMT: the material for fiber optical communication devices. Journal of Crystal Growth. 1 Jul 1985; 72(1-2): 490-5.

[47] Knight JC, Broeng J, Birks TA, Russell PS. Photonic band gap guidance in optical fibers. Science. 20 Nov 1998; 282(5393): 1476-8.

[48] Smith JM, Van Ness HC, Abbott MM, Swihart MT. Introduction to chemical engineering thermodynamics. Singapore: McGraw-Hill; 1949.

[49] Kaufman L, Cohen M. Thermodynamics and kinetics of martensitic transformations. Progress in Metal Physics. 1 Jan 1958; 7: 165-246.